ELSEVIER

Contents lists available at ScienceDirect

International Journal of Heat and Mass Transfer

journal homepage: www.elsevier.com/locate/ijhmt



Role of tissue porosity in thermal damage during microwave ablation

Teerapot Wessapan ^a, Pornthip Keangin ^b, Phadungsak Rattanadecho ^{c,*}, Nisakorn Somsuk ^d

- a Department of Mechanical Engineering, Faculty of Engineering, Rajamangala University of Technology Thanyaburi, Pathumthani 12110, Thailand
- b Department of Mechanical Engineering, Faculty of Engineering, Mahidol University, Nakhon Pathom 73170, Thailand
- ^c Center of Excellence in Electromagnetic Energy Utilization in Engineering (CEEE), Department of Mechanical Engineering, Faculty of Engineering, Thammasat University (Rangsit Campus), Pathumthani 12120, Thailand
- d Department of Industrial Engineering, Faculty of Engineering, Rajamangala University of Technology Thanyaburi, Pathumthani 12110, Thailand

ARTICLE INFO

Keywords: Microwave ablation (MWA) Thermal damage Porous media Tissue porosity Heat transfer

ABSTRACT

Microwave ablation (MWA) uses electromagnetic waves to produce localized heat for tumor therapy. This research examined the influence of tissue porosity on heat transmission and thermal damage patterns during microwave ablation via numerical simulations grounded in Maxwell's equations and porous media theory. Tissue necrosis was forecasted via an Arrhenius model, dependent on temperature and exposure time. The study findings show that higher tissue porosity leads to a more diffused and elongated necrotic zone due to enhanced convective heat transfer. The heightened porosity elevates fluid velocity and enhances natural convection currents, leading to a more comprehensive heat dispersion throughout the tissue, hence complicating the regulation of the tissue ablation zone and heightening the danger of harming healthy tissues. Moreover, higher microwave power levels intensify tissue heating and convection; when combined with intrinsic tissue porosity, this broadens heat dispersion and can distort the ablation-zone geometry. These observations underscore the necessity of accounting for tissue porosity in the optimization of MWA regimens. By customizing the microwave power level and exposure time to the porous nature of tissues, clinicians can predict thermal outcomes more accurately and improve tumor targeting while minimizing harm to the surrounding tissues. This approach is promising in realizing more precise and safer MWA treatments for cancer.

1. Introduction

In cancer treatment, minimally invasive therapies that eradicate tumors while preserving adjacent healthy tissues have been increasingly emphasized. In this regard, microwave ablation (MWA) is emerging as a pivotal technique that uses electromagnetic waves to generate localized thermal damage, thereby inducing necrosis in malignant cells [1]. For patients who are unable to undergo traditional surgery or radiation therapy, microwave ablation is particularly beneficial, as it has a lower risk of complications, a shorter recovery time, and is less invasive [2]. Careful targeting of tumor tissue can reduce recurrence rates and improve patient survival outcomes by carefully targeting tumor tissue while minimizing damage to surrounding healthy structures [3–5]. A thorough understanding of the parameters that affect the efficacy of microwave ablation, particularly the effects of thermal interactions in tissues, remains essential despite its increasing popularity. Thus, this study investigates the effect of tissue porosity on thermal damage.

Previous studies have demonstrated that tissue porosity is a key

factor in determining the temperature distribution in biological tissues during microwave ablation (MWA) [6]. The heat transfer of tissue ablation processes is significantly affected by porosity, which is characterized by the presence of small voids within the tissue structure [7]. These voids can enhance fluid movement in increasingly porous tissues. This results in significantly increased heat transfer [8]. Tissues with lower porosity tend to retain heat more efficiently, which may result in different thermal profiles after treatment [9]. Further research is needed to explore the relationship between these temperature fluctuations and heat damage. However, these findings are important for understanding the temperature dynamics in tissues during MWA. Understanding this relationship is crucial for a comprehensive understanding of how tissue porosity affects the severity of heat damage during MWA.

Mathematical modeling is essential to predict and understand the complex heat transfer processes that occur in biological tissues during thermal destructive treatments, such as microwave ablation (MWA). The Pennes bioheat equation and other classical models have been widely used to describe heat transfer in tissues [10]. However, these models have limitations in their applicability to tissues with different

E-mail address: ratphadu@engr.tu.ac.th (P. Rattanadecho).

 $^{^{\}ast}$ Corresponding author.

Nomenclatures		$arepsilon_p$	porosity (-)	
		κ	permeability (m ²)	
Α	frequency factor (1/s)	ho	density (kg/m³)	
C	specific heat capacity (J/(kgK))	ω	angular frequency (rad/s)	
d_p	effective pore diameter (m)	μ	dynamic viscosity (N.s/m²)	
E_a	activation energy (J/mol)	β	volume expansion coefficient (1/K)	
\overline{E}	electric field intensity (V/m)	λ	wavelength (m)	
g	gravitational acceleration (m/s ²)	k	propagation constant (m^{-1})	
$\overline{\overline{H}}$	magnetic field (V/m)	γ_0	free space wave number (m ⁻¹)	
i	identity matrix	$arepsilon_r$	relative permittivity (-)	
K	thermal conductivity $(W/(m \cdot K))$	$arepsilon_0$	permittivity of free space (F/m)	
P	input microwave power (W)	μ	relative permeability (-)	
p	pressure (Pa)	σ	electrical conductivity (S/m)	
Q	heat source (W/m ³)			
R	universal gas constant (J/(mol·K))	Subscri	•	
T	temperature (K)	b	blood	
t	time (s)	S	solid	
u	velocity (m/s)	met	metabolic	
Z	wave impedance (Ω)	ext	external	
	•	eff	effective	
Greek letters		ref	reference	
α	degree of tissue damage (-)	r	radial coordinate	
θ_d	fraction of tissue necrosis (-)	Z	axial coordinate	

porosity, as they may not adequately describe the complexity of heat transfer in such contexts. Porous media approaches, which characterize biological tissues as porous substances with interconnected voids, provide a more accurate picture of the thermal and fluid dynamics within the tissue. This strategy is more effective at capturing the complex interactions during thermal therapies and relies less on reducing assumptions. Khanafer and Vafai [11] emphasized the significance of porous media in biomedical engineering, particularly in relation to magnetic resonance imaging and drug delivery applications. Further, Khaled and Vafai [12] highlighted how porous media models more accurately capture the flow and heat transfer behavior in complex tissue structures compared to classical models. Mahjoob and Vafai [13] expanded on this by analytically detailing heat transport in biological media during hyperthermia, demonstrating that porous models provide more accurate predictions of tissue temperature and thermal damage.

Although previous research has emphasized the significant influence of tissue porosity on the temperature distribution in treated tissues, only a few studies have directly examined the relationship between porosity and the extent of thermal damage. Notably, Andreozzi et al. [14]. introduced a variable-porosity bioheat model that links heat transfer with tissue damage, highlighting the importance of incorporating porosity effects to improve thermal ablation accuracy. However, limited research has extended this approach to include the translation of temperature variation into tissue damage. The Arrhenius thermal damage model is important for this purpose, as it can predict tissue death depending on the temperature and duration of exposure [15]. However, very few studies have investigated the integration of this thermal damage model with porous media simulations to assess the effect of different porosity levels on thermal injury during MWA. To enhance the understanding of the influence of tissue porosity on the outcome of MWA therapy, this shortcoming needs to be addressed [16,17]. We have previously performed a comprehensive heat and mass transfer analysis in biological tissues exposed to an electromagnetic field. These include microwave [18-20], laser [21,22], and ultrasonic [23,24]. While our recent comparative study [29] contrasted HIFU and MWA in porous tissues, it did not systematically examine how porosity modulates thermal damage in MWA. The present work addresses this gap by focusing exclusively on MWA and varying tissue porosity (ε), treated as a prescribed, uniform control parameter, to quantify its effects on ablation-zone geometry, buoyancy-driven convection, and heat dispersion. These insights are intended to help refine MWA protocols. Using numerical models, the temperature distribution, prediction of tissue damage, and dynamics of fluid flow within porous media were examined. Subsequently, a robust framework was established to examine the interactions between thermal and electromagnetic fields and biological tissues.

This study employs a numerical model based on porous media theory to examine the effect of tissue porosity on thermal injury during MWA, thus providing a comprehensive analysis into the effect of porosity level on temperature distribution and thermal-injury magnitude based on simulated electromagnetic wave propagation, fluid dynamics, and heat transfer. This study integrates Maxwell's equations for electromagnetic wave propagation with transient momentum and energy equations to simulate the complex interactions between microwave energy and tissue structures. The Arrhenius-based thermal damage model predicts tissue necrosis based on temperature and exposure duration, thereby enabling accurate assessments of temperature distribution and thermal damage across varying tissue porosity levels during MWA. This study reveals the effect of porosity on thermal injury and provides critical insights into the associated heat-transfer mechanisms. These findings enhance our understanding regarding the interaction between tissue properties and microwave energy, thus offering valuable guidance for future clinical refinements of MWA.

2. Problem formulation

This study aims to enhance the accuracy and safety of MWA for the treatment of tumors. Despite the substantial potential of MWA for targeted cancer care, it is subject to certain constraints due to the potential for causing damage to contiguous healthy tissues that are impacted by the complex heat dynamics of tissues with varying porosities [6]. The extent of thermal injury and the distribution of heat during MWA are substantially influenced by tissue porosity, which is represented by microscopic voids [7]. The direct impact of tissue porosity on thermal injury is still largely unexplored, despite its significance. The objective of this study is to examine the impact of tissue porosity on thermal injury in MWA. Fig. 1 illustrates the MWA setup, where the microwave coaxial antenna delivers electromagnetic energy to the tumor, forming a

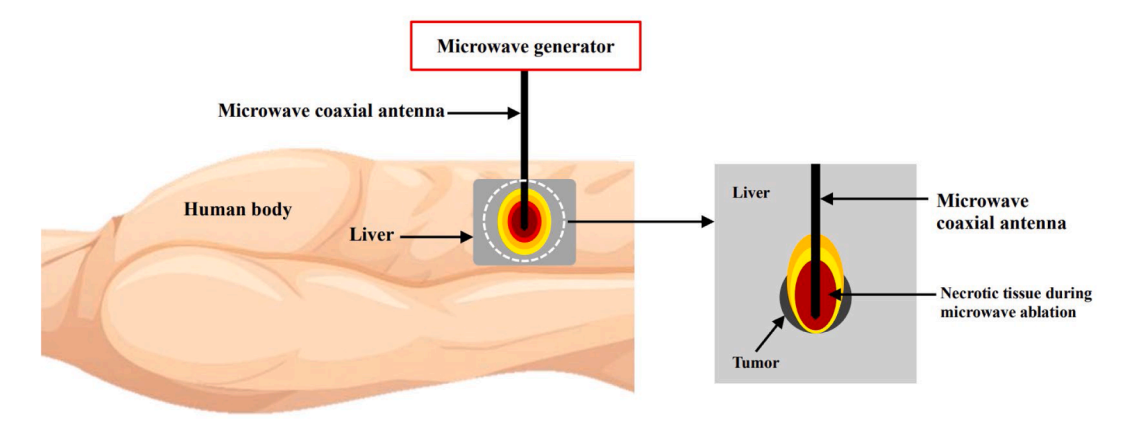


Fig. 1. Illustration of MWA system and necrotic zone.

necrotic zone. The simulation framework provides insights into heat transfer mechanisms, aiding treatment precision and safety. The antenna, which is powered by a microwave generator, concentrates electromagnetic energy on the tumor, thereby establishing a necrotic zone that can be used to ablate malignant cells. This configuration emphasizes the objective of MWA: to concentrate thermal injury on the tumor while preserving the healthy tissues in the vicinity.

3. Methods and model

The objective of this study was to examine the impact of tissue porosity on thermal injury during MWA through computational simulations. Consequently, the methods and models employed were specifically devised to achieve this objective. The primary goal is to comprehend the impact of tissue porosity on the absorption of energy, the transfer of heat, and the development of thermal injury in biological tissues. Initially, the distribution of absorbed energy within the designated tissue was determined by modeling electromagnetic wave propagation in porous tissues that were subjected to MWA [18]. Subsequently, an analysis was conducted to determine the impact of the absorbed microwave energy on the ensuing heat-transfer processes and the temperature increase, particularly in tissues with varying porosity levels. The effects of key parameters, such as tissue porosity levels, microwave power levels, and exposure periods, were systematically varied to evaluate their impact on thermal injury. The use of a two-dimensional (2D) axisymmetric model has been adopted to balance computational efficiency with physical accuracy, a common approach in similar MWA studies [18,23]. This model provides a practical compromise, enabling a detailed investigation of porosity effects while minimizing computational cost. The effects of evaporation and phase change were neglected in order to simplify the model. This assumption enables us to concentrate on the convection and heat conduction within porous tissues, thereby offering a more comprehensive understanding of the impact of porosity on thermal-damage patterns during MWA.

3.1. Physical model

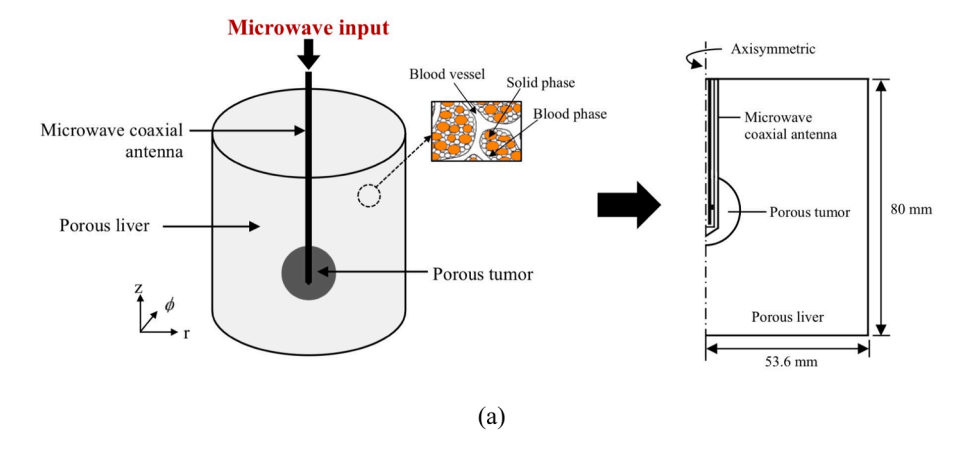
In this study, a fluid-filled porous tissue model was used to investigate the effect of porosity on the thermal characteristics during MWA. The model segments the tissue into vascular and extravascular regions, thus mimicking the actual biological structure during ablation. The tissue was assumed to be isotropic, with constant properties throughout, and was saturated with fluid to simulate the typical conditions in biological tissues. The dielectric properties ($\varepsilon_{\rm P}$, σ) for normal and tumor tissues were obtained from published data on liver tissue at 2.45 GHz [7, 23]. The porosity values were chosen based on literature and to assess a wide range of conditions, including higher values for sensitivity analysis. A uniform porosity assumption was applied to simplify the model.

In this work, tissue porosity (ε) is treated as a prescribed, spatially uniform control parameter within each tissue subdomain (tumor and surrounding parenchyma) and is varied systematically to isolate its effect on heating, flow, and lesion geometry. Temperature-, pressure-, or damage-dependent evolution of ε is not modeled and is left for future work. The tissue ablation model does not consider the main blood vessels or chemical interactions. The axisymmetric cylindrical coordinate system is applied under the assumption of rotational symmetry, ensuring that the physical processes and boundary conditions remain consistent in the radial direction. All simulations were performed in dimensional form, with parameters expressed in SI units to ensure consistency and facilitate comparison with experimental data. The tumor is shown as a 20 mm diameter sphere in the center of a larger cylindrical tissue region measuring 107.2 mm in diameter and 80 mm in height. The computational domain was chosen with sufficient distance between the tumor and the domain boundary to minimize boundary effects and avoid artificial reflections, ensuring an accurate representation of heat transfer and fluid dynamics. The tumor size and domain dimensions were selected based on established guidelines and previous studies [7,23,29]. To increase speed and precision, a two-dimensional (2D) axisymmetric model that presents a vertical slice of a three-dimensional (3D) model was used. This approach allows for a detailed analysis of the thermal effects while reducing the processing time. Such an assumption, frequently applied in numerical simulations, facilitates analysis and enhances computational efficiency while maintaining reasonable accuracy. This simplification has been validated in previous studies as an effective method to capture essential thermal effects with reduced computational effort. The physical model in Fig. 2 shows (a) a porous liver with a tumor and the location of a microwave coaxial antenna and (b) the single-slot antenna design, including the details of its structural components for targeted microwave energy delivery.

A microwave coaxial antenna measuring 1.79 mm [18] is placed at the core of the tumor to stimulate targeted electromagnetic waves and thermal distribution. The antenna is designed with a central conductor, an insulating dielectric layer, and an outer conductor. It includes a precisely crafted, 1 mm-wide, ring-shaped slot cut 5.5 mm from the short-circuit tip on the outer conductor, which is specifically designed for the effective targeting of deep-seated tumors. Operating at a frequency of 2.45 GHz, this configuration aligns with the standard MWA practices. Tables 1 and 2 list the properties of the tissue and the antenna used in the MWA simulations.

3.2. Wave propagation equations in MWA

The electromagnetic-wave movements investigated in this study were represented using 2D axially symmetric cylindrical coordinates (r, ϕ , z), which clearly expressed the interaction between the microwave energy and porous tissue throughout the ablation process. Starting from



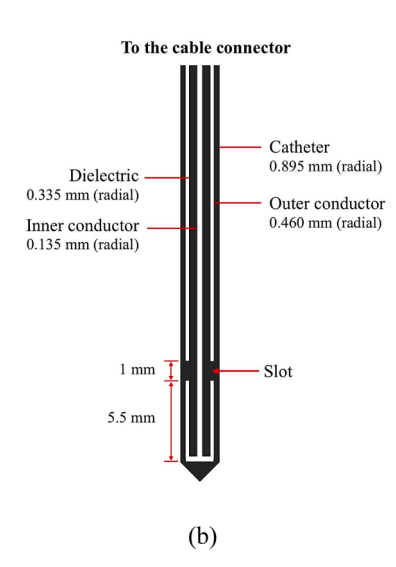


Fig. 2. Physical model used in this study: (a) Computational domain of problem investigated and (b) single-slot antenna.

Table 1Thermal and dielectric properties of biological tissues [23].

Normal tissue	Tumor	Blood
43	58.3	48.16
1.69	2.54	2.096
1030	1058	1040
3600	3960	3960
0.497	0.45	0.57
	43 1.69 1030 3600	43 58.3 1.69 2.54 1030 1058 3600 3960

the general form of Maxwell's equations in cylindrical coordinates under the time-harmonic assumption $e^{j\omega t}$, the simplifications are applied based on axisymmetric geometry and boundary conditions. The transverse electromagnetic (TEM) field efficiently captures the basic components of the electromagnetic wave as it traverses through a single microwave antenna slot. In the coaxial antenna region, the wave is modeled as a

TEM mode due to the axisymmetric boundary conditions, while upon exiting into the porous tissue, the field transitions into a transverse magnetic (TM) mode. The transition occurs due to the antenna's boundary conditions and the tissue's dielectric properties. Meanwhile, the transverse magnetic (TM) field effectively represents the dynamics of the electromagnetic wave as it traverses through the complicated network of porous tissues. The microwave antenna serves as a perfect conductor, thus preventing electric fields from reaching its walls. A scattering boundary was applied across the porous tissue's surface, which effectively truncated the computational domain and prevented artificial reflections. Although the domain is designed to minimize boundary reflections, the actual electromagnetic field distribution remains non-uniform due to tissue absorption and wave attenuation effects, which influence localized heating patterns. The time-varying TEM wave propagating along the microwave antenna was evaluated within this 2D axially symmetric framework to ensure a precise representation

Dimensions and dielectric properties of microwave coaxial antenna [18].

Materials	Dimensions (mm)	Dielectric properties	Dielectric properties			
		Relative permittivity, ε_r (-)	Electric conductivity, σ (S/m)	Relative permeability, μ (-)		
Inner conductor	0.135 (radial)	-	-	-		
Dielectric	0.335 (radial)	2.03	0	1		
Outer conductor	0.460 (radial)	-	-	-		
Catheter	0.895 (radial)	2.1	0	1		
Slot	1.000 (wide)	1	0	1		

of the electromagnetic fields. The electric and magnetic fields propagating along the antenna are expressed as follows [18]:

Electric field:

$$\vec{E} = e_r^{\ C} e^{i(\omega t - kz)} \tag{1}$$

Magnetic field:

$$\vec{H} = e_{\phi} \frac{C}{rZ} e^{j(\omega t - kz)},\tag{2}$$

where

$$C = \sqrt{\frac{ZP}{\pi \cdot \ln(r_{outer}/r_{inner})}} \tag{3}$$

In these equations, Z represents the wave impedance (Ω) ; P denotes the input microwave power (W); and r_{inner} and r_{outer} refer to the dielectric's inner and outer radii (m), respectively. Additionally, $\omega = 2\pi f$ is the angular frequency (rad/s), where f is the frequency (Hz), $k = 2\pi/\lambda$ is the propagation constant (m^{-1}) , and λ is the wavelength (m).

In porous tissues, electromagnetic waves are described using a TM field, which is appropriate for modeling the interaction of microwave energy within the tissue. The TM wave equation is derived by applying Maxwell's equations to the tissue region, considering the boundary conditions at the antenna-tissue interface and the scattering boundary at the outer domain, leading to the final simplified form shown in Eq. (4). The TM field formulation captures the essential behavior of electromagnetic waves as they propagate through the porous structure of the tissue, thus affecting the distribution of absorbed energy and the subsequent thermal effects [25]. The TM field in porous tissues is represented as follows:

$$\nabla \times \left(\left(\varepsilon_r - \frac{j\sigma}{\omega \varepsilon_0} \right)^{-1} \nabla \times \vec{H}_{\phi} \right) - \mu_r \gamma_0^2 \vec{H}_{\phi} = 0, \tag{4}$$

where ε_0 the permittivity of free space, whose value is 8.8542×10^{-12} F/m; ε_r is the relative permittivity (-); σ is the electric conductivity (S/m); μ_r is the relative permeability (-); and γ_0 is the free-space wave number (m⁻¹).

The TM wave propagated with strength fluctuations near the entry of the antenna, which simulated ablation. This TM wave formulation accounts for wave attenuation and phase shift caused by tissue properties such as permittivity ε_r , permeability μ_r , and conductivity σ , ensuring a realistic representation of microwave-tissue interactions. An axis symmetry at r=0 ensures uniform electromagnetic fields, which are essential for accurately modeling waves and their effect on tissue heating and damage.

3.3. Interaction between electromagnetic fields and human tissues

The specific absorption rate (SAR) defines the interaction between electromagnetic fields and human tissues and is a measure of the rate at which energy is absorbed by the tissue per unit mass. As electromagnetic waves pass through living tissues, they lose energy, which is absorbed and converted into temperature inside the biological material. Once the electric field distribution \vec{E} is determined from the TEM (Equations (1)–(3)) and TM (Equation (4)) solutions, its amplitude $|\vec{E}|$ is used in Equation (5) to compute the specific absorption rate (SAR). The SAR is the rate at which the tissue absorbs electromagnetic radiation. It represents both the exposure level and temperature reaction. The local SAR distribution determines the amount of energy converted into heat within the tissue and is calculated as the power dissipated per unit mass using the following formula:

$$SAR = \frac{\sigma}{\rho} \left| \vec{E} \right|^2, \tag{5}$$

where \vec{E} is the electric-field intensity (V/m), σ the electrical conductivity of the tissue (S/m), and ρ the tissue density (kg/m³).

The absorbed electromagnetic energy serves as a heat source within the tissue, contributing directly to temperature elevation. This heat generation can be expressed as:

$$Q_{\rm ext} = \sigma \left| \vec{E} \right|^2,\tag{6}$$

where $Q_{\rm ext}$ represents the heat source term induced by electromagnetic absorption, which directly influences the temperature distribution in the tissue.

3.4. Heat transfer and fluid flow equations in MWA

During MWA, microwaves penetrate the tissue, converting energy into heat, which leads to an increase in temperature. In order to comprehend the thermal and fluid behaviors in porous tissues during MWA, the effects of waves, fluids, and heat transfer are examined. To mitigate the complexity of the problem, the following assumptions are implemented:

- The thermal properties of the tissue remain constant throughout the operation.
- The tissue does not exhibit phase transition throughout the ablation process.
- 3. No chemical reactions occur within the tissue.
- 4. The tissue is represented as a fluid-saturated porous material that is thermally isotropic and homogeneous.

The LTE assumption was adopted to focus on the macroscopic thermal response of porous tissue during MWA while ensuring computational efficiency and ease of analysis. Although LTNE could improve accuracy in scenarios with rapid thermal gradients, its omission aligns with widely used modeling approaches and is supported by the validation results within the expected temperature range. In contrast to conventional biothermal models, the porous media approach is employed as a result of these assumptions, as it offers a more accurate representation of the transport phenomena in biological tissues. The model assumes biological tissue as a fluid-saturated porous medium, where the effective density accounts for both the solid matrix and interstitial fluid, ensuring a simplified yet representative formulation of momentum transfer. Although the Brinkman-extended Darcy model [26] effectively captures macroscopic transport phenomena in porous tissues, it does not explicitly resolve microscale heterogeneities such as individual capillary networks. Nonetheless, its use is justified in this study as it provides a computationally efficient approach to modeling coupled heat and fluid transport during MWA while maintaining reasonable accuracy. Permeability (κ) was not explicitly specified but was considered to vary with tissue porosity (ε) to ensure that the model accurately captures the coupled heat and fluid transport phenomena during MWA. The mathematical equations governing fluid transport inside a porous tissue are as

Continuity equation:

$$\nabla \cdot u = 0. \tag{7}$$

Momentum equation:

$$\left(\frac{\rho}{\varepsilon_p}\right)\frac{\partial u}{\partial t} + \left(\frac{\mu}{\kappa}\right)u = -\nabla p + \nabla \cdot \left[\left(\frac{1}{\varepsilon_p}\right)\left(\mu\left(\nabla u + \left(\nabla u\right)^T\right)\right)\right] + \rho g\beta\left(T - T_{ref}\right),\tag{8}$$

where ρ is the tissue density (kg/m³); κ is the tissue permeability (m²); u is the flow velocity (m/s); p is the pressure (Pa); μ is the dynamic viscosity (N.s/m²); T is the tissue temperature (°C); ε_p is the tissue porosity; T is the gravitational acceleration (m/s²); T is the volume expansion

coefficient (1/K); and T_{ref} is the reference temperature considered in this study, which is 37 °C. Buoyancy effects caused by temperature differences were modeled using the Boussinesq approximation, which assumes that the fluid density varies slightly with temperature but is unaffected by pressure. The primary driver of fluid flow in the porous tissue during MWA is thermal buoyancy and porosity-driven convection, rather than direct influence from the electromagnetic waves. The absorbed microwave energy contributes to heat generation, which induces temperature gradients that drive natural convection, particularly in regions with higher tissue porosity. As a result, the fluid motion is strongly influenced by the spatial distribution of heat and the permeability of the porous medium rather than by any direct electromagnetic force acting on the fluid.

In Eq. (8), the porosity term ε_p influences both the effective inertia and viscous effects, ensuring that reduced porosity leads to increased resistance to fluid movement. Additionally, permeability κ , which depends on ε_p , further controls the fluid flow, linking tissue structure to momentum transport.

In this work, permeability is modeled as a Kozeny–Carman function of porosity, consistent with Ref [7].:

$$\kappa(\varepsilon_p) = \frac{\varepsilon_p^3 d_p^2}{175 (1 - \varepsilon)^2},\tag{9}$$

where ϵ_p is porosity and d_p is the effective pore diameter. We set $d_p{=}1 \times 10^{-4}$ m (100 μ m) for all cases to isolate porosity effects.

The transient movement of thermal energy inside tissues is expressed as follows:

Energy equation [29]:

$$(\rho C)_{\it eff} \frac{\partial T}{\partial t} - \nabla \cdot \left(K_{\it eff} \nabla T \right) = -(\rho C)_b u \cdot \nabla T + Q_{\it met} + Q_{\it ext}, \tag{10}$$

where

$$(\rho C)_{eff} = (1 - \varepsilon_p)(\rho C)_s + \varepsilon_p(\rho C)_b \tag{11}$$

is the overall heat capacity per unit volume of the tissue, and

$$K_{eff} = (1 - \varepsilon_p)K_s + \varepsilon_p K_b \tag{12}$$

Here, $(\rho C)_{\rm eff}$ represents the overall heat capacity per unit volume of the tissue, $K_{\rm eff}$ the effective thermal conductivity of the tissue (W /m·K), ρ the density of the tissue (kg/m³), T the tissue temperature (°C), t the time (s), $C_{\rm eff}$ the effective heat capacity (J/kg·K), $Q_{\rm met}$ the metabolic heat generation (W/m³), and $Q_{\rm ext}$ the external heat source (W/m³). The subscripts eff, s, and b correspond to the effective value, solid-tissue phase, and blood phase, respectively.

In this study, parameters defining the limitations of thermal transmission and fluid flow were selected to represent the actual heat and fluid dynamics within the tissue model during MWA. Key parameter values, including tissue porosity, microwave power levels, and exposure times, were carefully chosen to reflect realistic biological conditions. Assumptions, such as constant tissue properties and the absence of phase transitions, were also clearly defined to ensure the accuracy and relevance of the model. The temperature of the tissue exterior surface was fixed at 37 °C in the simulation, thus ensuring a uniform thermal environment surrounding the tissue. For the flow study, open boundaries were introduced outside the model boundaries, thus allowing the fluid to propagate freely inside and outside the computational domain. The initial fluid velocity was set to zero to reflect the absence of forced flow, and buoyancy-driven flow was modeled using the Boussinesq approximation to capture natural convection effects. The initial temperature throughout the model was set to 37 °C, thus providing a consistent baseline temperature for the simulation.

3.5. Thermal-Damage equation

The Arrhenius equation was used to quantify the level of thermal damage in the tissues caused by MWA. The thermal damage parameter, $\alpha(t)$, was computed as the integral of the Arrhenius equation [27] as follows:

$$\alpha(t)_{eff} = \int_{0}^{t} A e^{\frac{-E_{a}}{RT}} dt \tag{13}$$

In this equation, α represents the degree of tissue damage, where A (1/s) is the frequency factor, and E_{α} (J/mol) is the activation energy required for the irreversible damage reaction. Both parameters are tissue specific and vary depending on the biological material being modeled. The constant R is the universal gas constant, whose value is 8.314 (J/mol.K), and T is the absolute temperature (K) within the tissue. This integral accounts for the accumulation of energy in the tissue over time, thus enabling a detailed prediction of the thermal-damage extent. In this study, the values used were $A = 1.18 \times 10^{44}$ (1/s) and $E_{\alpha} = 3.02 \times 10^{5}$ (J/mol), as adopted from [27]. These values were used in thermal ablation modeling for hepatic tissues and have been referenced in previous studies for predicting microwave-induced damage in liver tissue.

The parameter α is typically related to the fraction of tissue necrosis θ_d , which can be calculated as follows:

$$\theta_d = 1 - e - \alpha \tag{14}$$

This relationship provides a clear representation of the extent of tissue necrosis based on the computed thermal damage, α . The thermal-damage equation is crucial for predicting the effectiveness and safety of MWA, as it allows one to determine the level of tissue destruction during the procedure.

3.6. Calculation procedure

In order to resolve the intricate governing equations and boundary conditions, the finite-element method (FEM) was implemented in this investigation. This method guarantees high precision and efficiency in numerical simulations by dynamically revising the mesh density in response to location-specific and temporal differences in the solution, utilizing an adaptive mesh-refining technique. COMSOL™ Multiphysics was employed to simulate the complex thermal and electromagnetic phenomena that occur within the tissue model during MWA in order to implement and execute these calculations. Adaptive time-stepping was applied to enhance accuracy and stability while optimizing computational efficiency. An axisymmetric finite-element model was employed to conduct simulations, which effectively represented the 3D characteristics of the problem and optimized the computational resources. Second-order Lagrange elements were used for discretization, ensuring a balance between accuracy and efficiency. The porous tissue was initially maintained at 37 °C, which is the core-body temperature. The FEM's accuracy was ensured by conducting a mesh-independence test, as illustrated in Fig. 3. The solution's independence from the lattice density was demonstrated by the fact that the maximal temperature remained constant as the number of elements exceeded 12,000. The mesh independence study primarily evaluated the maximum temperature to ensure both numerical stability and computational efficiency, which is a widely adopted approach in similar studies for thermal analysis in MWA simulations.

4. Results and discussion

This section provides a thorough examination of the impact of tissue porosity on the thermal injury sustained during MWA. The heat-transfer dynamics and thermal-damage extent were comprehensively evaluated by conducting simulations across a variety of tissue-porosity levels, power inputs, and exposure periods. Throughout the simulation, it was

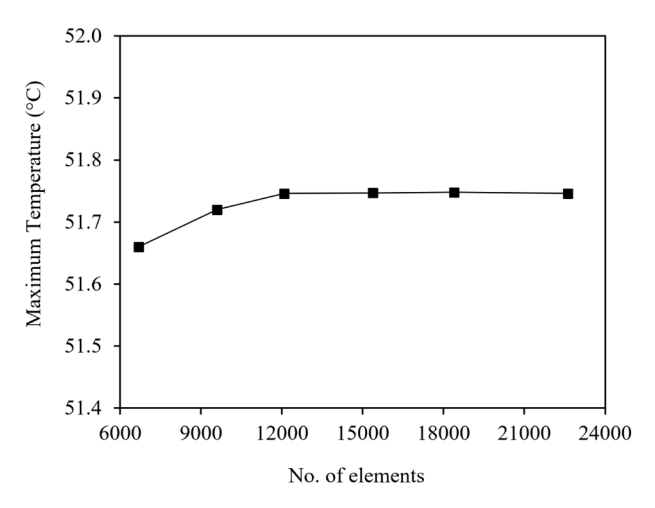


Fig. 3. Mesh-independence test results of model.

supposed that the porous tissue's properties would remain constant. The results were consistent with clinical scenarios by modeling the properties of the tissue and microwave antenna based on previously established data [18,23], as illustrated in Tables 1 and 2. The main findings and implications for enhancing the precision and efficacy of MWA in cancer treatment are underscored by the model's validation and subsequent discussions.

4.1. Model validation

A validation study was conducted to verify the model's accuracy by comparing the simulation results with data obtained from Yang et al. [28]. during MWA treatment. The temperature increase within the model is illustrated in Fig. 4 for two distinct radial distances from the antenna (4.5 and 9.5 mm). The validation data were derived from ex vivo experiments on bovine liver tissue conducted by Yang et al. [28]., where temperature measurements were taken under controlled conditions. The study employed a 2.45 GHz microwave source with specific power settings, and temperature sensors were placed at designated radial positions to capture transient thermal responses. These experimental conditions closely align with the assumptions of our numerical model, ensuring meaningful comparison. In our validation simulation, the liver was modeled as a homogeneous porous tissue with uniform porosity ε =0.3. The corresponding permeability κ was obtained from the Kozeny-Carman relation (Eq. (9)). The numerical model's ability to effectively capture the heat-transfer dynamics within porous liver tissue

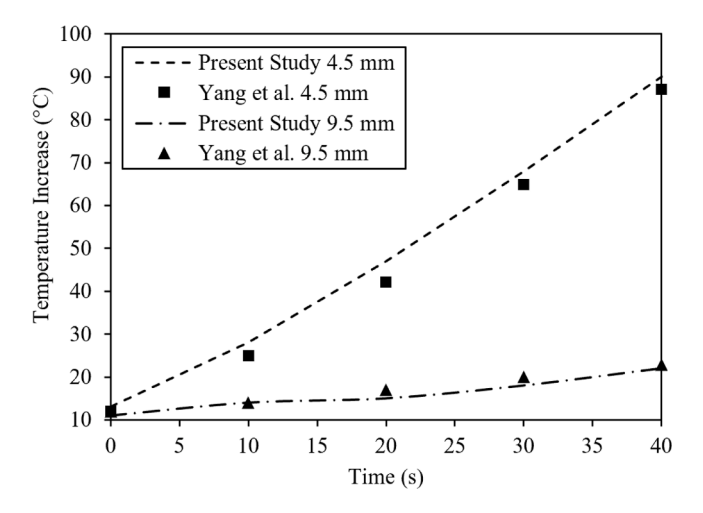


Fig. 4. Results showing validation of hepatic-tissue temperature, compared with experimental data obtained from Yang et al. [28]. during MWA treatment.

was validated by the fact that the simulation results of the present study closely aligned with the data reported by Yang et al. for both distances. The focus on temperature validation provides a direct assessment of the heat transfer process, which is a critical factor influencing tissue response during MWA. The model's capacity to reliably forecast the temperature during MWA is illustrated by the accord between the numerical results and published data. The close agreement between the simulated and measured temperature profiles indirectly supports the accuracy of the Arrhenius-based thermal damage predictions, as the computed temperature field serves as the input to the damage model. This validation reinforces the model's applicability for examining the impact of tissue porosity and microwave power on thermal damage.

4.2. Spatial distribution of SAR

The SAR profiles for tissues with a porosity of $\varepsilon = 0.1$ are depicted in Fig. 5 at varying microwave power levels. The rate at which electromagnetic radiation is absorbed by tissues per unit mass is critical in determining the thermal pattern during MWA, as indicated by the SAR. The energy distribution within the tissue is represented by the color gradients in the figure, with regions of greater energy absorption indicated by areas with higher SAR. Concentrated around the antenna, the maximal SAR value (SAR_{max}) was 9460.6 W/kg at 5 W. SAR_{max} increased to 18,921 and 28,382 W/kg, respectively, as the microwave power increased to 10 and 15 W, respectively, with the absorption extending further into the tissue. This pattern suggests that the region of considerable energy absorption is expanded, and the peak SAR values are increased as a result of higher microwave power levels. The microwave energy increased in a restricted region directly around the antenna, as indicated by the spatial distribution of the SAR. Nevertheless, the SAR distribution appeared to become more elongated as the power increased, indicating that the ablation zone may be extended by higher power levels. The energy field's extension at greater power levels enables a more extensive treatment area, which can be beneficial for targeting larger tumor masses. However, it must be closely monitored to prevent damage to the adjacent healthy tissues.

4.3. Temperature distribution and thermal-damage progression

Fig. 6 illustrates the temperature distribution, fluid-flow patterns (streamlines), and scope of necrotic tissue during MWA at 15 W for exposure durations of 30, 60, and 120 s. The temperature increased gradually, as illustrated in Fig. 6a, and attained a maximal value (T_{max}) of 97.11 °C at 120 s. The streamlines, which depict the flow of fluid within the tissue, demonstrate the manner in which the heated regions influence natural convection. As the temperature increased, the fluid propagated away from the central tumor zone. The tumor region was modeled with a lower porosity (ε =0.1) compared to the surrounding normal tissue (ε =0.3), leading to restricted fluid infiltration within the tumor. This results in the fluid streamlines observed in Fig. 6a, which flow around the tumor rather than through it, creating recirculation zones that enhance convective heat transfer in the surrounding tissue. The heat distribution was significantly improved by this convective flow, particularly as the exposure time increased. Furthermore, Fig. 6b illustrates the extent of thermal damage, with red denoting complete necrosis, blue denoting no damage, and intermediate colors representing varying degrees of partial necrosis. The tumor, which is the primary objective of MWA, is symbolized by the central circular zone. For subsequent quantification, the necrosis boundary is delineated by the Arrhenius contour $\alpha = 1$, from which longitudinal (axial) and transverse (radial) diameters are measured. Notably, at 15 W and 120 s, higher porosity produces reduced axial elongation and a small upward centroid shift, consistent with stronger buoyancy-driven convection (see Section 4.4).

The SAR is essential for the temperature escalation depicted in Fig. 6a, as evidenced by the comparison of the SAR patterns in Fig. 5. At

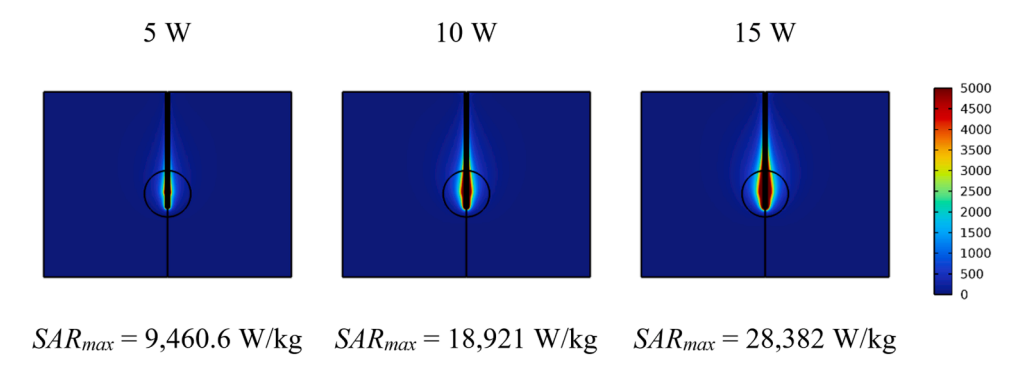


Fig. 5. SAR profiles yielded by developed model at different microwave power levels based on tissue porosity of 0.1.

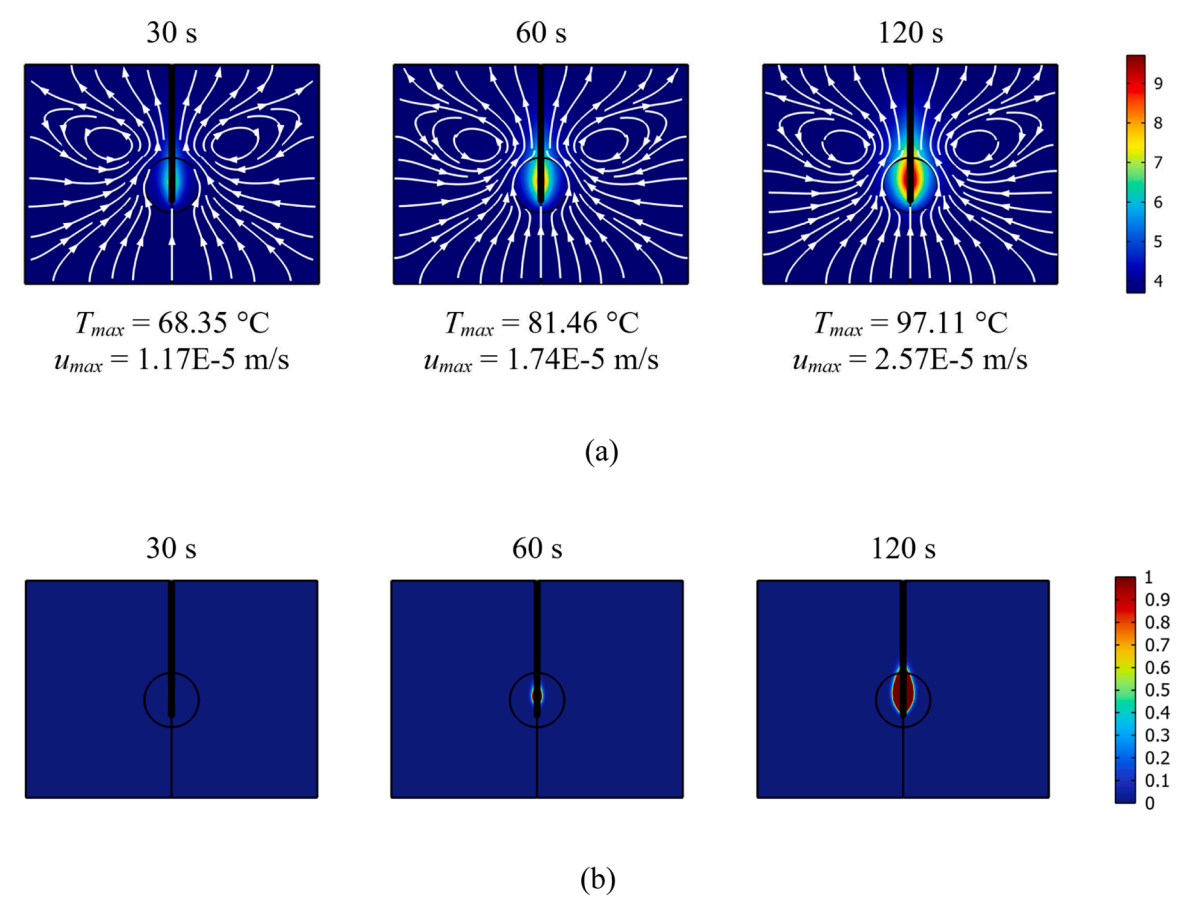


Fig. 6. Temperature profiles and fraction of necrotic tissue at microwave power level of 15 W and at different exposure times: (a) temperature profiles within tissue after 30, 60, and 120 s; the streamlines indicate fluid flow around the tumor due to its lower porosity (ε =0.1) compared to the surrounding tissue (ε =0.3), which restricts fluid penetration and promotes recirculation; (b) necrotic tissue within tissue after 30, 60, and 120 s of MWA.

15 W, the SAR, which is indicative of the energy absorption rate within the tissue, attained its maximal value of 28,382 W/kg. The higher temperatures depicted in Fig. 6a are indicative of the fact that the tissue assimilated a greater amount of energy, which in turn generated a greater amount of heat. For example, the SAR produced a maximal temperature of 81.46 °C (T_{max}) at 60 s, which resulted in limited thermal injury that was primarily restricted to the tumor area, as illustrated in Fig. 6b The majority of the tissue remained unaffected during the initial stage of ablation, which exhibited a moderate heat distribution. The streamlines in Fig. 6(a) illustrate the velocity field derived from the momentum equation (Eq. (8)). As tissue porosity decreases ($\varepsilon = 0.1$), infiltration is restricted, causing flow to bypass the tumor and form recirculation zones in the surrounding tissue. This convective effect significantly influences the spatial distribution of temperature, as

highlighted in Fig. 7, where higher power levels lead to increased fluid velocity and enhanced heat transfer. The streamline patterns in Fig. 7 demonstrate how lower porosity of tumor restricts fluid flow, causing localized heat accumulation and creating a compact necrotic zone, whereas higher porosity facilitates broader convective heat transfer, modulating lesion geometry—at 15 W and 120 s we observe modest radial broadening, axial shortening, and a slight upward displacement of the necrosis centroid (Fig. 8c; see Section 4.4).

The relationship between the SAR, temperature, and thermal damage became more evident as the exposure duration increased. An increase in fluid velocity contributed to more efficient heat transfer, resulting in a temperature increase area. This led to an expanded necrotic zone, as illustrated in Fig. 6b, in which the ablation affected both the tumor and certain adjacent tissues. By 120 s, the temperature

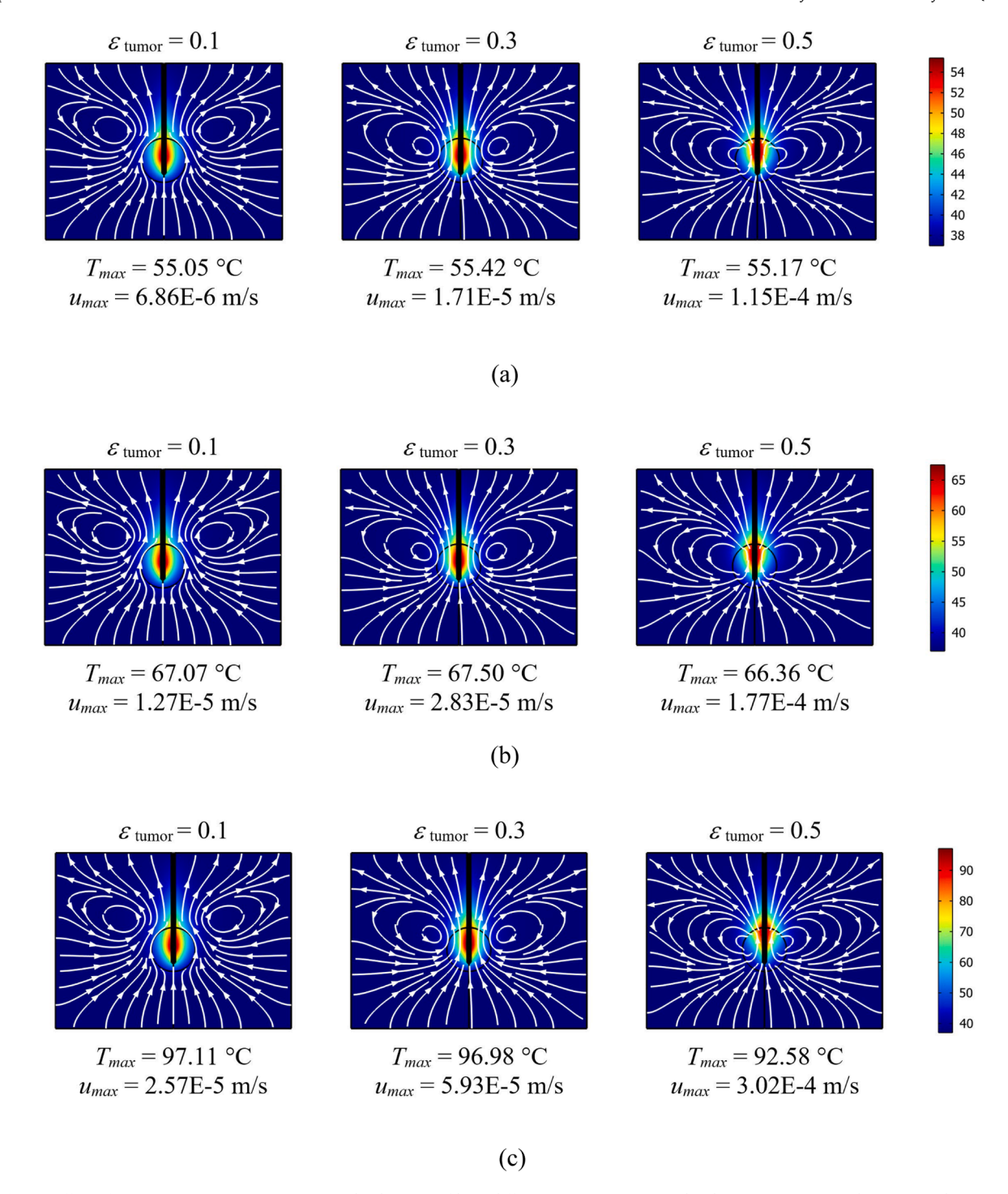


Fig. 7. Effect of tissue porosity on temperature and velocity profile at different microwave power levels at 120s: (a) 5 W, (b) 10 W, and (c) 15 W.

had reached 97.11 °C, and the SAR continued to enhance the thermal effect. The necrotic area that corresponded to the tumor zone experienced a substantial expansion and extended beyond it. This emphasizes the importance of closely monitoring these parameters to ensure effective ablation while minimizing collateral damage, as higher SAR values and protracted exposure times lead to more extensive tissue destruction.

4.4. Effects of tissue porosity and microwave power on temperature distribution and necrosis

Figs. 7 and 8 illustrate the impact of tissue porosity and microwave power on the heat distribution, fluid movement, and tissue necrosis that

are observed during MWA. The temperature and velocity profiles in Fig. 7 demonstrate that the maximum temperature (T_{max}) and maximum fluid velocity (u_{max}) in the vicinity of the tumor region were substantially increased as the microwave power increased. At 120 s, the maximum temperature increase was moderate at a power level of 5 W, with modest fluid velocities and a T_{max} of 55.05 °C. Nevertheless, the maximum temperature (T_{max}) increased significantly to 97.11 °C when the power was increased 15 W with a porosity of 0.1. The streamlines in the figure suggest that the natural convection was facilitated by higher power levels, which led to a more pronounced fluid circulation around the heated tumor zone and the efficient distribution of heat throughout the tissue.

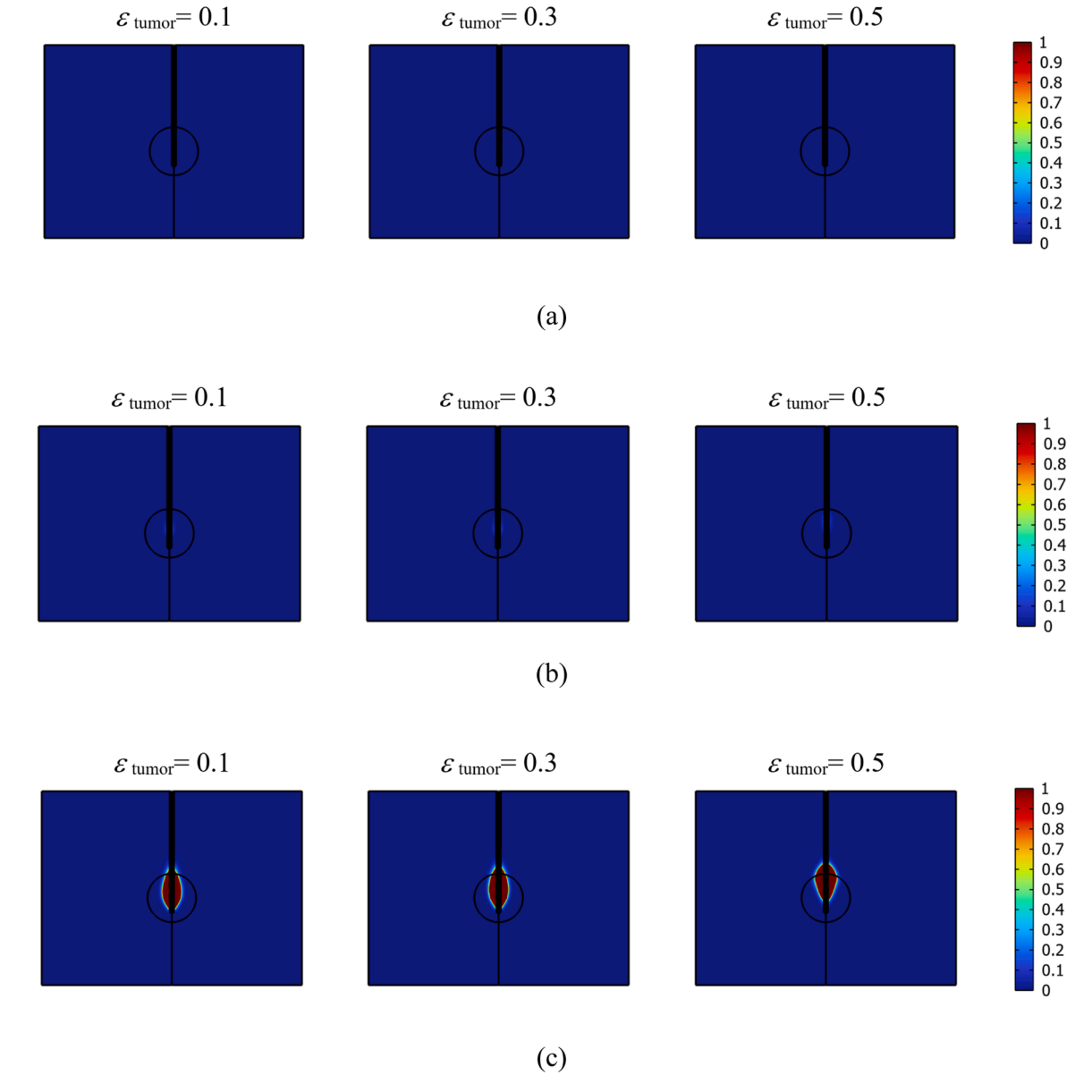


Fig. 8. Effect of tissue porosity on necrotic-tissue fraction at different microwave power levels at 120s: (a) 5 W, (b) 10 W, and (c) 15 W.

The extent of tissue necrosis was found to be correlated with both the microwave power and tissue porosity, as demonstrated in Fig. 8. No thermal injury was observed at 5 W for 120 s, despite the temperature increase depicted in Fig. 7, across all porosity levels. At 10 W, a small necrotic region began to emerge, particularly in cases with lower porosity, as illustrated in Fig. 8. At 15 W, the necrotic zone significantly extended beyond the tumor region, as illustrated in Fig. 8(c). Quantitatively (15 W, 120 s), the $\alpha=1$ necrosis contour gives D_{trans}/D_{long} of 7.8/15.6 mm for $\varepsilon = 0.1$ and $\varepsilon = 0.3$, and 8.8/14.4 mm for $\varepsilon = 0.5$, where D_{trans} is the transverse (radial) diameter and D_{long} is the longitudinal (axial) diameter. Between $\varepsilon = 0.1$ and 0.3 the geometry is essentially unchanged; at $\varepsilon = 0.5$ the lesion is wider transversely and shorter axially (lower aspect ratio), with a slight upward centroid shift. The rise in porosity enhanced natural convection and fluid dynamics, leading to an expansion of the thermal damage zone. This effect corresponds with the velocity profiles presented in Fig. 7, indicating that increased porosity levels are associated with elevated fluid velocities, thereby facilitating enhanced heat transfer and the distribution of necrotic tissue. These results align with previous studies [6,7], but our results uniquely highlight the role of enhanced fluid convection in

reshaping the necrotic zone during MWA. The final extent and morphology of thermal injury during MWA are determined by the relationship among tissue porosity, fluid flow, temperature profiles, and microwave power.

The effects of tissue porosity and microwave power on the temperature increase and necrotic-tissue fractions at specific locations within the tissue are further examined in Figs. 9 and 10, which continue the analysis of tissue responses during MWA. These figures evaluate two monitoring points on the mid-plane along the radial line through the antenna: P1 at r=5 mm and P2 at r=10 mm. In Fig. 9, the impact of varying tissue porosity ($\varepsilon=0.1$, 0.3, and 0.5) at a constant microwave power of 15 W is illustrated. In Fig. 10, the impact of varying microwave power levels (5,10, and 15 W) at a fixed tissue porosity of 0.1 is illustrated. By comparing these findings with the temperature and necrosis patterns depicted in Figs. 7 and 8, a comprehensive understanding of the spatial and temporal dynamics of thermal injury during MWA was obtained.

As shown in Fig. 9a, at point P1, which is located 5 mm from the microwave antenna, the temperature increased rapidly, particularly at lower tissue porosity levels. Under a porosity of $\varepsilon = 0.1$, the temperature

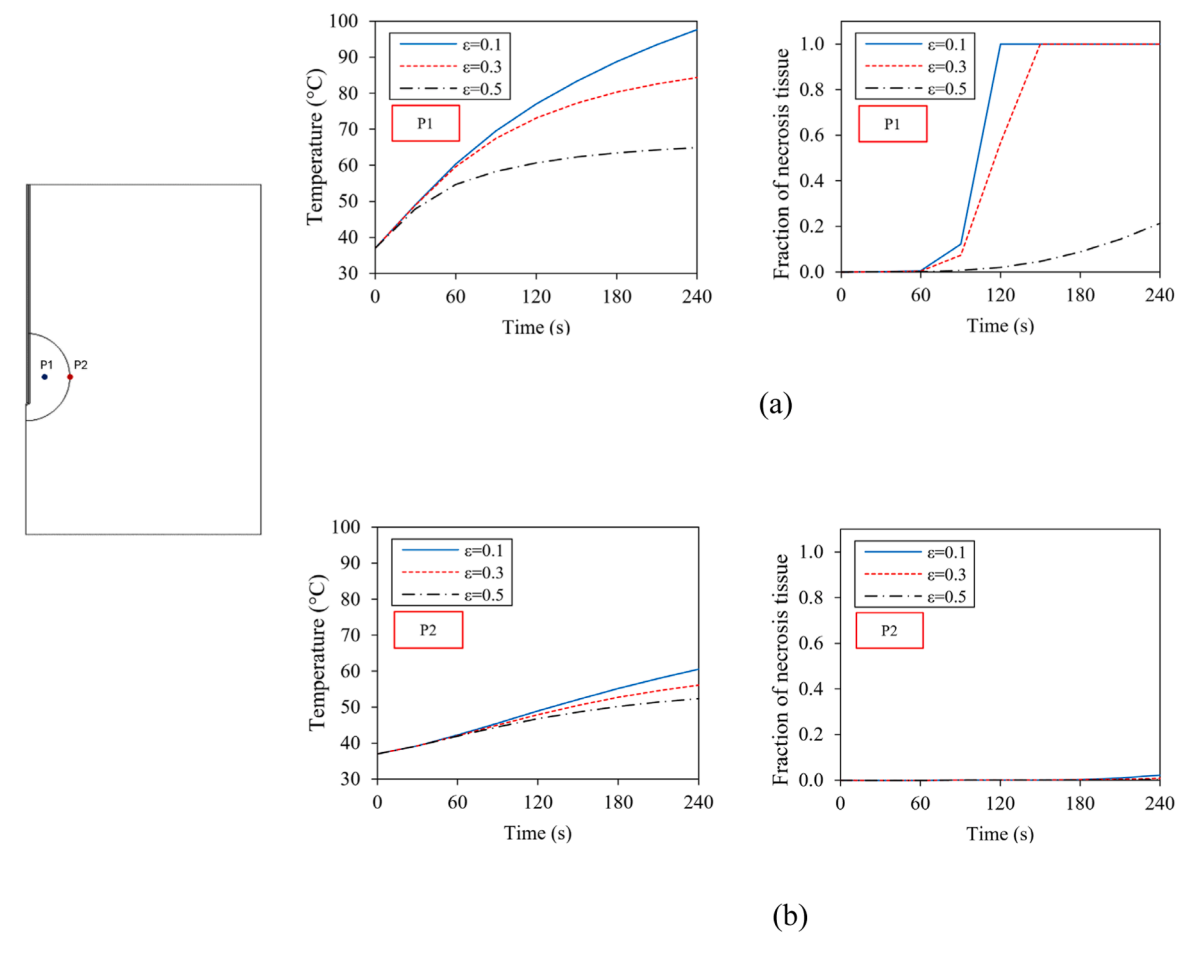


Fig. 9. Temperature increase and necrotic-tissue fraction at 15 W for tumor porosities $\varepsilon = 0.1, 0.3, 0.5$: (a) P1 (r = 5 mm) and (b) P2 (r = 10 mm).

reached approximately 95 °C within 200 s, thus resulting in a complete necrosis immediately after 120 s, as indicated by the necrotic-tissue fraction reaching 1. At higher porosity levels ($\varepsilon=0.3$ and 0.5), a more gradual temperature increase and delayed necrosis onset were indicated, thereby reflecting the moderating effect of increased porosity on heat accumulation due to enhanced fluid convection and heat dispersion. At point P2 (see Fig. 9b), which is located at the edge of the tumor, the temperature increased more gradually across all porosity levels, and the progression of necrosis was significantly delayed. At the highest porosity ($\varepsilon=0.5$), necrosis was negligible even after 240 s, thus corroborating the observations from Figs. 7 and 8 that higher porosities facilitate broader but less intense heating effects, particularly at greater distances from the energy source.

Fig. 10 complements these findings by demonstrating the impact of microwave power on necrosis and temperature at a constant tissue porosity of 0.1. The temperature increase was more pronounced at point P1 (refer to Fig. 10a) due to the higher microwave power, with 15 W leading to a more rapid rise and accelerated tissue necrosis. Meanwhile, lower power levels (5 and 10 W) resulted in delayed necrosis and slower temperature increases, highlighting the direct correlation between microwave power and thermal-damage progression. At site P2 (refer to Fig. 10b), the temperature increased gradually at all power levels, but the highest power level of 15 W was the only one that exhibited significant necrosis after extended exposure periods. This spatial variability is consistent with the temperature and necrosis profiles depicted in Figs. 7 and 8. The necrotic zone was expanded, particularly in the vicinity of the antenna, at higher microwave power levels, while the necrotic area was restricted at lower power levels.

Integrating the findings of Figs. 9 and 10 with earlier observations

underscores the critical relationship among tissue porosity, microwave power, and spatial positioning within the tissue in determining the thermal outcomes during MWA. Lower porosity and higher microwave power intensified the thermal effects near the antenna, thus resulting in rapid and localized necrosis, as evidenced by the swift temperature increase at point P1. Conversely, higher porosity and lower power levels promoted heat dispersion owing to enhanced fluid convection, thus resulting in slower temperature increases and more diffused necrosis, particularly at points farther from the energy source, such as P2. These findings highlight the necessity to fine-tune the MWA settings by considering tissue characteristics and treatment goals to improve tumor elimination while sparing neighboring healthy tissues.

5. Conclusions

A sophisticated mathematical model was used in this study to examine the effect of tissue porosity on thermal injury during MWA. The findings demonstrate that tissue porosity significantly affects the temperature distribution and thermal-damage extent within a tumor and its surrounding tissues. Higher tissue porosity enhanced fluid convection, thus resulting in broader heat dispersion and a more extensive necrotic zone. This complicated the restriction of the ablation zone to the target and increased the potential for incidental harm to normal tissues. Additionally, variations in microwave power interact with intrinsic tissue porosity to shape the thermal response and necrotic patterns observed during MWA, often promoting anisotropic heat spread and elongating the ablation-zone geometry. At higher porosity levels ($\varepsilon = 0.5$), the necrotic region became more diffuse and elongated, extending further into the surrounding tissues compared to lower porosity cases (ε

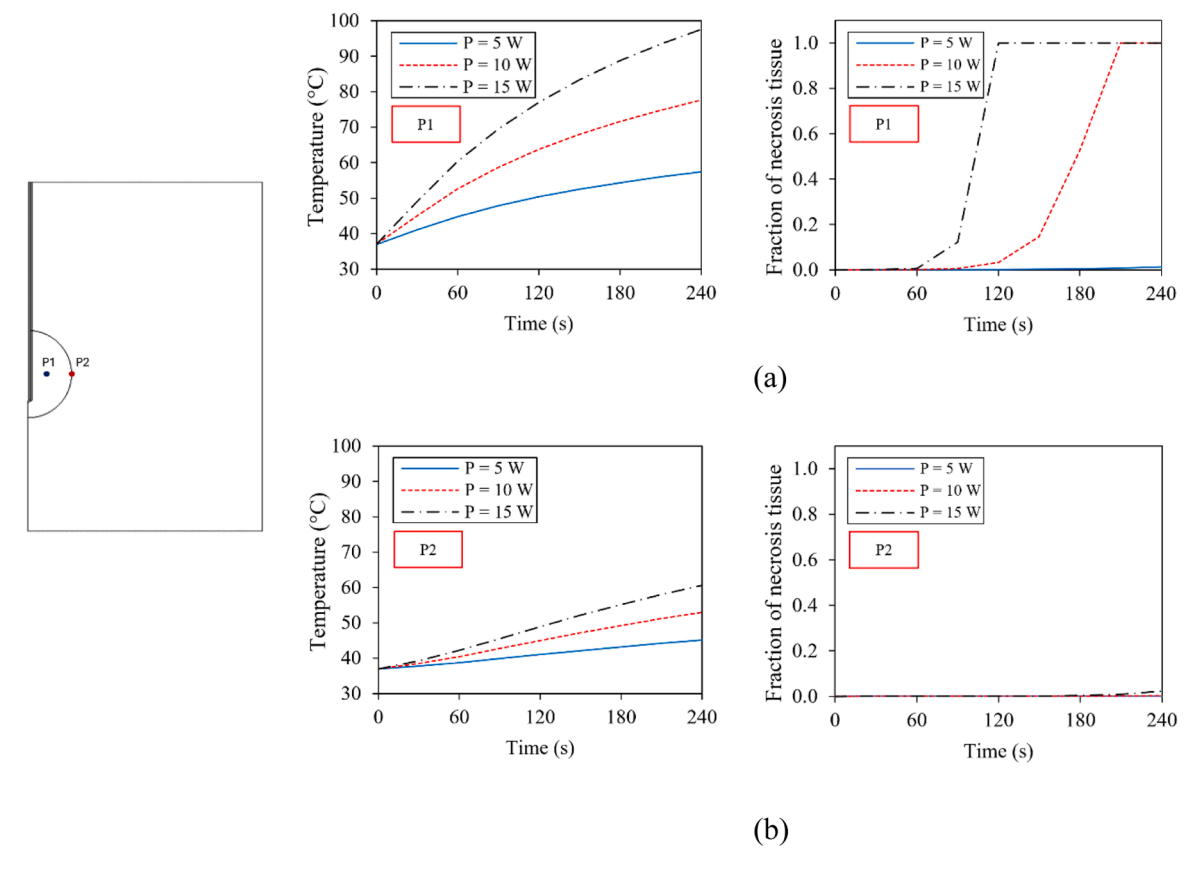


Fig. 10. Temperature increase and necrotic-tissue fraction at different microwave power levels based on tissue porosity of 0.1: (a) At p1 and (b) p2.

= 0.1), where the damage remained more localized. This effect was particularly pronounced at 15 W, where the necrotic fraction was significantly higher in highly porous tissues due to enhanced convective heat transfer.

These findings underscore the importance of considering tissue porosity when planning and optimizing MWA procedures. By considering the porosity of the targeted tissue, clinicians can predict the thermal behavior more accurately and adjust the microwave power levels and exposure times accordingly. Future studies should focus on the development of personalized MWA protocols that incorporate patient-specific tissue properties, including porosity, to improve the precision and safety of tumor-ablation therapies. Such advancements can result in more effective cancer treatments with fewer side effects, thus ultimately improving patient outcomes.

CRediT authorship contribution statement

Teerapot Wessapan: Writing – review & editing, Writing – original draft, Project administration, Investigation, Funding acquisition, Conceptualization. **Pornthip Keangin:** Validation, Methodology, Data curation. **Phadungsak Rattanadecho:** Supervision, Funding acquisition. **Nisakorn Somsuk:** Writing – review & editing, Resources.

Declaration of competing interest

Please declare for each author any conflicts of interest relevant to what you write. This includes employment, consultancies, stock ownership, honoraria, paid expert testimony, patent applications and travel grants. If there are no conflicts of interest, please state that there are The authors declare that they have no known competing financial interests or personal relationships that could have appeared to influence the work reported in this paper.

Acknowledgments

This research was supported by the National Science, Research, and Innovation Fund, Thailand Science Research and Innovation (TSRI), through Rajamangala University of Technology Thanyaburi (FRB67E0707) (Grant no. FRB670027/0168). The authors gratefully acknowledge the Thailand Science Research and Innovation Fundamental Fund for the fiscal year 2024, 2025 and the National Research Council of Thailand (Grant Number N42A650197).

Data availability

The authors do not have permission to share data.

References

- N.H. Shaheen, A.D. Hardie, Approach to hepatic tumor ablation: choosing the right tool for the job, Acad. Radiol. (2024), https://doi.org/10.1016/j. acra.2024.02.034.
- [2] W. Yao, X. Du, Study of microwave ablation in patients with unresectable soft tissue sarcoma, J. Clin. Oncol. (2023), https://doi.org/10.1200/jco.2023.41.16_ suppl.e23545.
- [3] M. Ahmed, C.L. Brace, F.T. Lee, S.N. Goldberg, Principles of and advances in percutaneous ablation, Radiology 258 (2) (2011) 351–369.
- [4] S.N. Goldberg, C.J. Grassi, J.F. Cardella, J.W. Charboneau, G.D. Dodd, D.E. Dupuy, et al., Image-guided tumor ablation: standardization of terminology and reporting criteria, Radiology 235 (3) (2005) 728–739.
- [5] C.L. Brace, Microwave ablation technology: what every user should know, Curr. Probl. Diagn. Radiol. 39 (2) (2010) 61–67.
- [6] M. Xin, N. Wu, Q. Nan, S. Bi, Simulation study of microwave ablation of porous lung tissue, Appl. Sci. 13 (2023) 625, https://doi.org/10.3390/app13010625. -625
- [7] P. Rattanadecho, P. Keangin, Numerical study of heat transfer and blood flow in two-layered porous liver tissue during microwave ablation process using single and double slot antenna, Int. J. Heat Mass Transf. 58 (1–2) (2013) 457–470.
- [8] J.L. Hernandèz, A. Kim, W. Woodrow, Medical applications of porous biomaterials: features of porosity and tissue-specific implications for biocompatibility, Adv. Heal Mater. (2022), https://doi.org/10.1002/adhm.202102087.

- [9] Y. Tang, Y. Wang, R.C.C. Flesch, T. Jin, Effect of porous heat transfer model on different equivalent thermal dose methods considering an experiment-based nanoparticle distribution during magnetic hyperthermia, J. Phys. D (2023), https://doi.org/10.1088/1361-6463/acc07d.
- [10] H.H. Pennes, Analysis of tissue and arterial blood temperatures in the resting human forearm, J. Appl. Physiol. 1 (2) (1948) 93–122.
- [11] K. Khanafer, K. Vafai, The role of porous media in biomedical engineering as related to magnetic resonance imaging and drug delivery, Heat Mass Transf. 42 (2006) 939–953.
- [12] A.R. Khaled, K. Vafai, The role of porous media in modeling flow and heat transfer in biological tissues, Int. J. Heat Mass Transf. 46 (2003) 4989–5003.
- [13] S. Mahjoob, K. Vafai, Analytical characterization of heat transport through biological media incorporating hyperthermia treatment, Int J Heat Mass Transf. 52 (2009) 1608–1618.
- [14] A. Andreozzi, L. Brunese, M. Iasiello, C. Tucci, G.P. Vanoli, A new thermal damagecontrolled protocol for thermal ablation modeled with modified porous mediabased bioheat equation with variable porosity, Processes 10 (2022) 236.
- [15] E.M. Ahmed, G.D. Noojin, M.L. Denton, Damage integral and other predictive formulas for nonisothermal heating during laser exposure, J. Biomed. Opt. 27 (3) (2022) 035001, https://doi.org/10.1117/1.JBO.27.3.035001.
- [16] G. Shankar, E.P. Siva, D. Tripathi, O.A. Beg, Thermal analysis in unsteady oscillatory Darcy blood flow through stenosed artery, Int. J. Thermofluid. 24 (2024) 100864, https://doi.org/10.1016/j.ijft.2024.100864.
- [17] A. Andreozzi, L. Brunese, M. Iasiello, C. Tucci, G.P. Vanoli, A new thermal damage-controlled protocol for thermal ablation modeled with modified porous media-based bioheat equation with variable porosity, Processes 10 (2) (2022) 236, https://doi.org/10.3390/pr10020236.
- [18] P. Keangin, P. Rattanadecho, T. Wessapan, An analysis of heat transfer in liver tissue during microwave ablation using single and double slot antenna, Int. Commun. Heat Mass Transf. 38 (6) (2011) 757–766.
- [19] T. Wessapan, P. Rattanadecho, Temperature induced in the testicular and related tissues due to electromagnetic fields exposure at 900 MHz and 1800 MHz, Int. J. Heat Mass Transf. 102 (2016) 1130–1140.

- [20] D. Bhargava, P. Rattanadecho, T. Wessapan, The effect of metal objects on the SAR and temperature increase in the human head exposed to dipole antenna (numerical analysis). Case Studies in Thermal Engineering, 2020, p. 22.
- [21] P. Wongchadakul, P. Rattanadecho, T. Wessapan, Implementation of a thermomechanical model to simulate laser heating in shrinkage tissue (effects of wavelength, laser irradiation intensity, and irradiation beam area), Int. J. Therm. Sci. (2018), https://doi.org/10.1016/J.IJTHERMALSCI.2018.08.008.
- [22] P. Wongchadakul, P. Rattanadecho, T. Wessapan, Simulation of temperature distribution in different human skin types exposed to laser irradiation with different wavelengths and laser irradiation intensities, Songklanakarin J. Sci. Technol. 41 (3) (2019) 529–538.
- [23] T. Wessapan, P. Rattanadecho, Flow and heat transfer through a porous tumor during high-intensity focused ultrasound, Int. J. Heat Mass Transf. 216 (2023) 124501.
- [24] T. Wessapan, P. Rattanadecho, Acoustic streaming effect on flow and heat transfer in porous tissue during exposure to focused ultrasound, Case Stud. Therm. Eng. 21 (2020) 100670.
- [25] J.M. Bertram, D. Yang, M.C. Converse, Antenna design for microwave hepatic ablation using an axisymmetric electromagnetic model, Biomed. Eng. Online 5 (2006) 15.
- [26] H.C. Brinkman, A calculation of the viscous force exerted by a flowing fluid on a dense swarm of particles, Appl. Sci. Res. A 1 (1949) 27–34.
- [27] M. Selmi, A. Bajahzar, H. Belmabrouk, Effects of target temperature on thermal damage during temperature-controlled MWA of liver tumor, Case Studies in Thermal Engineering, 2022. https://doi.org/10.1016/j.csite.2022.101821.
- [28] D. Yang, M. Converse, D. Mahvi, Expanding the bioheat equation to include tissue internal water evaporation during heating, IEEE Trans. Biomed. Eng. 54 (8) (2007) 1382–1388
- [29] T. Wessapan, P. Keangin, P. Rattanadecho, N. Somsuk, Comparative analysis of heat transfer dynamics in high-intensity focused ultrasound and microwave ablation for cancer treatment, Int. J. Thermofluid. 26 (2025) 101090.